Research Paper

EARTHQUAKE SPECTRA

Three-dimensional 0–10 Hz physics-based simulations of the 2020 Magna, Utah, earthquake sequence

Earthquake Spectra
2025, Vol. 41(2) 1177–1199

DOI: 10.1177/87552930241307797
journals.sagepub.com/home/eqs
Sage

Ke Xu, M.EERI[1,2], Kim Bak Olsen[1], and Te-Yang Yeh, M.EERI[1]

Abstract
Earthquakes on the Salt Lake City Segment of the Wasatch fault (WFSLC) represent the most significant seismic hazard to the Salt Lake Valley, populated by 1 million + people. The 2020 Magna, UT, earthquake, which likely occurred on the WFSLC, generated peak ground accelerations (PGAs) as large as 0.55 *g* in the Salt Lake Valley. Here, we present three-dimensional (3D) physics-based wave propagation simulations of the Magna earthquake sequence in the Wasatch Front Community Velocity Model (WFCVM) up to 10 Hz to better constrain both linear and nonlinear parameters in the soils of the Salt Lake Valley. We first calibrate the WFCVM via linear simulations of a M_w4.59 Magna aftershock, obtaining the best fit between the recordings and synthetics, including a statistical distribution of small-scale heterogeneities with 10% standard deviation and $Q_S = 0.05V_S$ for frequencies <1 Hz and $Q_S = 0.05V_S f^{0.4}$ for frequencies >1 Hz (V_s in m/s). Spectral ratios from our simulations of the 2020 Magna mainshock using a finite-fault source model generally overestimate those for the recordings in the linear regime at higher frequencies, in particular at stations with the largest PGAs, suggesting the presence of nonlinear soil effects. Using a fully hysteretic multi-yield-surface 3D nonlinear modeling approach, we find that damping from the reference strain–depth relations proposed by Darendeli significantly reduces the bias in terms of spectral amplification ratios at stations with the shortest epicentral distances. We find an optimal fit between the recordings and nonlinear synthetics for reference strains at about 2 standard deviations below Darendeli's relations, with reduction of the spectral amplification bias by more than a factor of two. Our findings suggest significant nonlinear soil effects in the Salt Lake Valley and provide a basis for improved seismic hazard analysis of the greater Salt Lake City region.

[1]Department of Earth & Environmental Sciences, San Diego State University, San Diego, CA, USA
[2]Scripps Institution of Oceanography, University of California San Diego, San Diego, CA, USA

Corresponding author:
Ke Xu, Department of Earth & Environmental Sciences, San Diego State University, 5500 Campanile Dr, San Diego, CA 92182, USA.
Email: kxu4143@sdsu.edu

Keywords
Salt Lake Valley; Wasatch fault; physics-based simulation; wave propagation; nonlinear soil response

Date received: 19 June 2024; accepted: 22 November 2024

Introduction

Earthquake hazards in the Salt Lake Valley are a serious concern because the valley is a major urban center with a population of more than one million people. The most prominent source of seismic hazard to the Salt Lake Valley is the Salt Lake City segment of the Wasatch fault (WFSLC), a major normal fault that separates the Salt Lake basin from the Wasatch Mountains to the east (DuRoss, 2008; Machette et al., 1991, 1992). Paleoseismological studies of the Salt Lake City segment indicate that large, above M7, surface faulting earthquakes have occurred on average every 1350 $\pm$ 200 years during the last 6000 years along this segment, with the most recent event 1230 $\pm$ 60 years ago (Black et al., 1995; DuRoss et al., 2016; McCalpin and Nelson, 2000; McCalpin and Nishenko, 1996). Based on this information, McCalpin and Nelson (2000) estimated the probability of such an event occurring during the next 100 years to be about 16% and Wong et al. (2002) estimated the probability during the next 50 years to be 6% to 9%. Other faults and fault segments, such as the West Valley fault, the Great Salt Lake fault, the northern Oquirrh fault, and the Provo and Weber segments of the Wasatch fault, also contribute significantly to the seismic hazard in the Salt Lake Valley, along with "background" earthquakes of $M \leqslant 6.5 \pm 0.25$ (e.g. Wong et al., 2002; Youngs et al., 2000). As a result, Salt Lake City has an annual estimated loss of 174 million dollars and is ranked number five out of metro areas with the highest seismic risk in the United States (Jaiswal et al., 2023).

As the most recent M7 event occurred long before the advent of instrumental seismic recordings, physics-based wave propagation simulations provide the most promising tool to constrain the expected ground motions for future large earthquake scenarios on the Wasatch fault. Physics-based ground motion simulations for frequencies up to 1 Hz have been carried out in the Salt Lake Valley by incorporating local velocity models and kinematic source models for M7 scenarios (Moschetti et al., 2017; Roten et al., 2011). Parker et al. (2023) used a crossed mixed-effect analysis on the three-dimensional (3D) M7 WFSLC simulations by Roten et al. (2011) and Moschetti et al. (2017) and found that directivity effects dominated the ground motion variability in the resulting Ground Motion Model (GMM), and recommended the direct use of the simulations themselves (Parker et al., 2023). Roten et al. (2012) extended the bandwidth for the M7 WFSLC simulations up to 10 Hz by merging deterministic simulations with stochastic scattering functions, and used a simple nonlinear soil model derived from laboratory tests of a few samples of Bonneville Clay obtained in the Salt Lake basin (Bay and Sasanakul, 2005). Roten et al. (2012) clearly showed that nonlinear soil effects in the Salt Lake Valley will play a significant role for a large Wasatch Fault earthquake.

The 18 March 2020, Magna, Utah, earthquake sequence, which caused $629 million in total economic losses related to buildings (https://earthquakes.utah.gov/magna-quake/) in the Salt Lake Valley and several minor injuries to local residents (Pankow et al., 2020) was the largest recorded earthquake in the Salt Lake Valley since a similar magnitude event occurred in 1962 in the same area (Kleber et al., 2020). The Magna earthquake sequence produced an unprecedented seismic data set, as its main shock and 34 M_w>3 aftershocks were recorded by the densely distributed University of Utah Seismograph Stations (UUSS) network near the epicenter (University of Utah, 2020a). The magnitude of the mainshock was estimated at $M_w5.7$ from Saint Louis University (2020) moment tensor solutions and $M_w5.5$ from University of Utah (2020b); here, we adopt the latter solution. The mainshock (with peak ground accelerations (PGAs) up to 0.54 g) is the first well-recorded event generating ground motions capable of triggering nonlinear effects in the Salt Lake Valley. The overprediction of PGAs and spectral accelerations by a leading GMM (Abrahamson et al., 2014) suggests the presence of nonlinear effects at the closest soil stations (Wong et al., 2021). Here, we use these recorded ground motions to better constrain the properties of basin sediments, including the velocity model parameters and nonlinear soil rheology in the Salt Lake Valley, using 3D seismic ground motion simulations with a hysteretic nonlinear, multi-yield-surface method (Roten et al., 2023) up to 10 Hz.

The article is organized as follows: We first describe the numerical modeling method and the 3D velocity model used in our study. Then, the model features, including anelastic attenuation, near-source basin structure, small-scale heterogeneities, finite-fault source model, and reference strains in the nonlinear soil rheology, are validated based on the simulations of an aftershock and the mainshock in the 2020 Magna sequence. Finally, we discuss uncertainties in our results and provide recommendations for future work.

Numerical modeling method

We used the fourth-order staggered-grid finite-difference code AWP-ODC (with suffix derived from the authors, Olsen, Day, and Cui) for our simulations of the 2020 Magna earthquakes. AWP-ODC has been highly optimized on GPU platforms (Cui et al., 2013), with support for modeling nonlinear soil effects via a multi-yield-surface (Iwan-type) 3D approach (Roten et al., 2023). The code provides support for a discontinuous mesh with a factor-of-three change in grid spacing along mesh blocks in the vertical dimension (Nie et al., 2017), as well as statistical distributions of small-scale heterogeneities (SSHs, Savran and Olsen, 2016). In addition, AWP-ODC supports frequency-dependent anelastic attenuation implemented as a power-law following Withers et al. (2015):

$$Q(f) = Q_0\left(\frac{f}{f_0}\right)^{\gamma},\ f \geqslant f_0, \tag{1}$$

where Q_0 is a constant Q value specified separately for P (Q_P) and S (Q_S) waves, f_0 is the upper frequency of constant Q, which is fixed as 1.0 Hz in our simulations, and γ controls Q for frequencies above f_0. We used $Q_P = 2Q_S$ following Brocher (2008). While AWP-ODC has support for topography, this feature was not available at the time of this project. For this reason, the simulations are carried out using a flat free surface boundary condition (Gottschämmer and Olsen, 2001).

To simulate nonlinear soil effects, we use the multi-surface, 3D model incorporated into AWP-ODC by Roten et al. (2023). In this method, a large number of spring sliders (Kaklamanos et al., 2015) are combined using the overlay concept (Iwan, 1967; Mróz, 1967). For each spring slider representing a von Mises yield surface that is associated with a pre-calculated yield level, the material follows elastic, perfectly-plastic behavior. The hysteretic behavior dictated by the Masing rule (Masing, 1926) is facilitated by the spring sliders arranged in a parallel-series configuration. Convergence of the method is obtained for 7–10+ yield surfaces (Kaklamanos et al., 2015; Roten et al., 2023). In this Iwan-type

Table 1. Model parameters used for the ground motion simulations of the 2020 Magna earthquakes

Models	Linear	Nonlinear (near-fault)
E-W dimension	36.45 km	18.00 km
N-S dimension	24.30 km	24.30 km
Southwest corner	(–112.18, 40.605)	(–112.18, 40.605)
Depths (bottom of three blocks)	2.32 km / 2.77 km / 24.30 km	
Grid discretization (three blocks)	2.5 m / 7.5 m / 22.5 m	
Number of total spatial grids	~134 billion	~66 billion
Minimum V_s	125 m/s	
Points per minimum wavelength	5	
Maximum frequency	10 Hz	
Number of GPU processors	1350	4500
Wall-clock time	3.5 h	12 h
Time discretization	0.00027 s	
Simulation time	32.4 s	21.6 s
Number of time steps	120,000	80,000

model, the nonlinear response of the soil is described by the reduction of the shear modulus of the uniaxial simple shear as

$$\frac{G}{G_0} = \frac{1}{1 + \frac{\gamma_{xy}}{\gamma_r}}, \tag{2}$$

where γ_r is the reference strain, γ_{xy} is shear strain, and G_0 is the maximum shear modulus. The reference strain is defined as

$$\gamma_r = \frac{\tau_0}{G_0}, \tag{3}$$

where τ_0 is the yield stress, the maximum shear stress that the material can support under the initial stress state (Roten et al., 2012). τ_0 can be calculated through the cohesion (C) and the friction angle (ϕ) as

$$\tau_0 = C \cdot cos(\phi) - (\sigma_m - P) \cdot sin(\phi), \tag{4}$$

where P is the fluid pressure, and σ_m is the effective mean stress. For simplicity, we used the lithostatic stress as a proxy for σ_m in the calculation of yield stress.

Velocity model

For our wave propagation simulations in the Salt Lake basin, we use the 3D Wasatch Front Community Velocity Model (WFCVM) version 3d (Magistrale et al., 2008). The WFCVM is constructed based on basin sediment categories, basement depths, near-surface low-velocity material within the basin, and crustal velocities for surrounding regions down to Moho and the upper mantle, from various data sets including geologic surveys, geotechnical borehole velocity logs, and seismic tomography results. We extracted a rectangular computational domain along E-W and N-S for the central Salt Lake Valley to a depth of 24.3 km. The parameters used in our numerical simulations are listed in Table 1, where we applied a discontinuous mesh with three blocks and a minimum V_s of 125 m/s (see also Figure S1). Figure 1 shows our modeling domains (dashed rectangle in (b) for a smaller

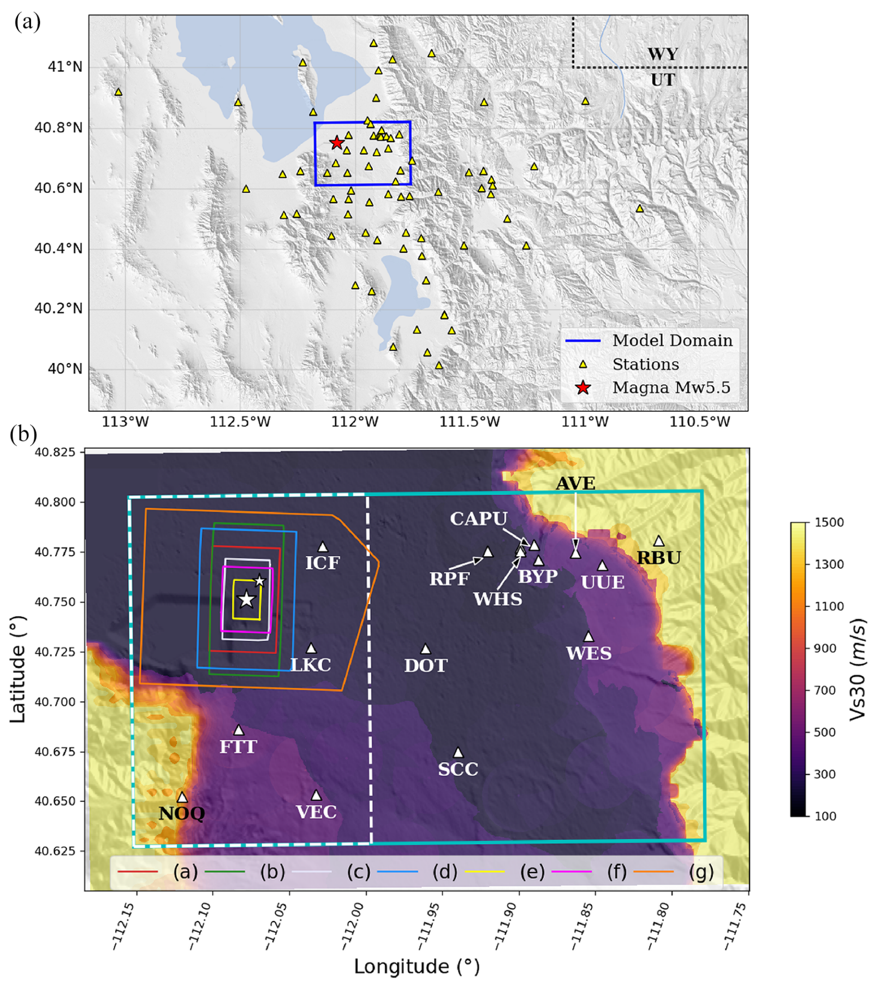

Figure 1. Maps of the model regions, with topography shown by shading (not included in the simulations). (a) Regional map containing our Salt Lake Valley models, with triangles showing all available stations within a 100 km epicentral distance range from the M_w4.59 aftershock. (b) V_{s30} within the rectangle in (a), obtained from the WFCVM version 3d (Magistrale et al., 2008). The epicenters of the 2020 Magna mainshock (large) and the M_w4.59 aftershock (small) are depicted by stars. Seismic stations are shown by triangles, where NOQ and RBU are permanent stations on rock. The outermost solid rectangle outlines the region used for the validation simulations in the linear regime, and the dashed rectangle depicts a smaller domain used for the nonlinear simulations. The colored polygons near the epicenters outline the surface projections of our seven-candidate finite-fault rupture models for the Magna main shock (see Figure 8).

near-source domain in our nonlinear modeling), seismic station coverage, and the location of the epicenters of the Magna mainshock and M_w4.59 aftershock. Figure 1b shows V_{s30} from the WFCVM. A majority of the central-eastern Salt Lake basin consists of unconsolidated sediments with V_{s30} below 250 m/s (including sites ICF and LKC), while the southwestern area is characterized by V_{s30} values in the range 300–600 m/s, where FTT is located. The mountains are described by V_{s30}~1400 m/s in the WFCVM, with rock sites NOQ to the west and RBU east of the basin.

Goodness-of-fit measures

We use the Olsen and Mayhew (2010) Goodness-of-Fit (GOF) criteria to evaluate the fit between our simulations and seismic recordings, which includes 10 different metrics in the time and spectral domains. As some of these metrics are highly correlated (see Olsen and Mayhew, Figure 8), we have selected four metrics with lower correlation for our analysis, namely, PGA, peak ground velocity (PGV), 5%–95% duration (DUR), and Fourier Spectra (FS) within specified bandwidths of the simulations and data. Olsen and Mayhew defined classifications of "poor" (35–45), "fair" (45–65), "very good" (65–80), and "excellent" (80–100).

In addition to the Olsen and Mayhew (2010) GOF measures, we use the bias of the Fourier acceleration spectra (FAS), geometrically averaged for a total of N_s stations:

$$\varepsilon_{FAS}(f) = \overline{\left\{ \frac{\mathcal{F}[A_{syn}](f)}{\mathcal{F}[A_{obs}](f)} \right\}} \Bigg|_{N_s,\, geom}, \tag{5}$$

where A_{syn} and A_{obs} are the synthetic and observed time series, respectively, which are both band-pass filtered between 0.1 and 10.0 Hz, and $\mathcal{F}$ denotes calculation of Fourier amplitude spectra, which are all smoothed by a first-order Savitzky–Golay filter (Savitzky and Golay, 1964) and a 31-point window length.

Validation of the WFCVM

We first validated our extraction of the WFCVM against observations from the largest aftershock (M_w4.59) in the 2020 Magna sequence which has a well-constrained moment tensor solution inverted from seismic recordings by UUSS (Pang et al., 2020; University of Utah, 2020b). Nonlinear effects tend to increase with frequency, where the PGA threshold for the onset has been estimated to be near $0.1g$ (Beresnev and Wen, 1996; Kaklamanos et al., 2013; Rajaure et al., 2017). We limit the validation simulations to the linear regime, since the PGA values recorded at the 16 stations in the modeling region during the selected aftershock are $0.12g$ or smaller.

Aftershock source description

We used a point source approximation for the aftershock, characterized by a minimum-phase slip rate time function, which are calculated from Brune's (1970) ω^{-2} source spectral model as

$$\Omega(t; f_c) = (2\pi f_c)^2 t \exp[-2\pi f_c t] H(t), \tag{6}$$

where t is time, $H(t)$ is the Heaviside step function, and f_c is the corner frequency determined by

$$f_c = 0.49 V_s \left(\frac{\Delta\sigma}{M_0} \right)^{\frac{1}{3}}, \tag{7}$$

where M_0 is the scalar moment in N·m, V_s is the shear velocity at the point source in m/s, and $\Delta\sigma$ is the stress drop in Pa, following Brune's model for S waves.

Table 2. Source locations and moment tensor solutions for the mainshock and largest (M_w4.59) aftershock in the Magna, Utah, earthquake sequence from Pang et al. (2020) and University of Utah (2020b). Event times listed are UTC time on 18 March 2020

Event time	Strike – Dip – Rake (°)	Depth (m)	Hypocenter (°W,°N)	M_0 (dyne · cm)	M_w
13:09:31 (Main)	(182, 34, –52)	9000	(112.078, 40.751)	2.316×10^{24}	5.54
14:02:12	(179, 34, –61)	9070	(112.069, 40.760)	8.494×10^{22}	4.59

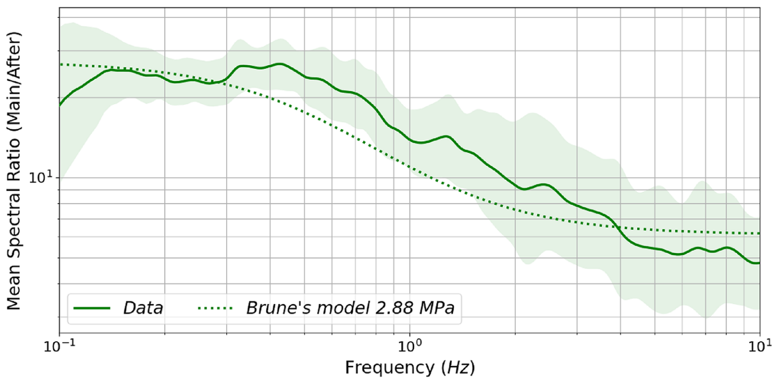

Figure 2. Spectral ratio of the Magna mainshock relative to the M_w4.59 aftershock, averaged from 51 available stations (see Figure 1a). The dotted ratio shows the best-fit Brune's model. Color shading depicts $\pm 1\sigma$ of the averaged spectrum.

We estimated the corner frequencies for the aftershock through averaged spectral ratios, to eliminate site effects and estimate the stress drop of the aftershock relative to the mainshock. The spectral ratio between the mainshock and aftershock can be estimated as

$$\frac{\Omega^m(f)}{\Omega^a(f)} = \frac{M_0^m}{M_0^a} \cdot \frac{1 + \left(f/f_c^a\right)^2}{1 + \left(f/f_c^m\right)^2}, \tag{8}$$

where f_c^a and f_c^m are corner frequencies for the aftershock and the mainshock, respectively, which are related to the corresponding stress drop $\Delta\sigma^a$ or $\Delta\sigma^m$ through Equation 7, assuming that both the mainshock and aftershock follow Brune's (1970) source model. We used least-squares optimization of the spectral ratios for the observations and simulations to estimate the best-fitting corner frequency model, averaging the horizontal components of recordings at 51 stations within a hypocentral distance of 100 km (see Figure 1a), filtered between 0.1 and 10 Hz. We found an optimal stress drop ($\Delta\sigma$) of 2.88 MPa for the M_w4.59 aftershock (see Figure 2), which is used in our validation simulations. Additional source parameters are adopted from Pang et al. (2020), see Table 2.

Anelastic attenuation and lower velocity taper parameters

Hu et al. (2022) showed that incorporating near-surface low-velocity material (here, labeled a low-velocity taper, LVT) into the Statewide California Earthquake Center

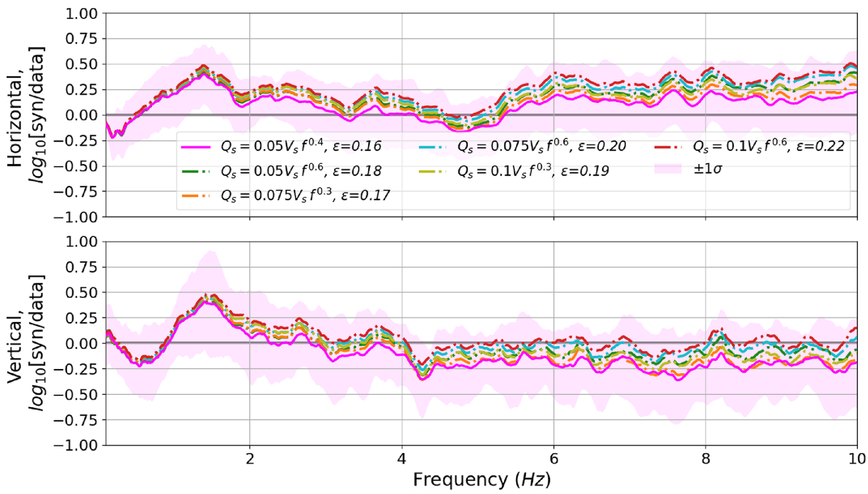

Figure 3. Comparison of FAS bias log_{10}(synthetics/data) for the M_w4.59 aftershock (see Table 2) averaged across 16 stations with PGA <0.12 g (see Figure 1b for locations) with different anelastic attenuation parameters. The magenta curve shows the preferred model with optimal fit ($Q_S = 0.05V_S f^{0.4}$), the color shading depicts the $\pm 1\sigma$ range of the station-wide average from the preferred model, and the E values in the legend depict the three-component averaged absolute error in log scale.

CVM-S4.26.M01 improved the fit to the seismic data for the 2014 M5.1 La Habra earthquake, due to unrealistically large V_s at sites outside the basins. The LVT is constrained by a V_{s30} value, as well as the tapering depth, where the LVT merges with the profiles from the WFCVM (as described by the approach by Ely et al. (2010), see Equation S4 in the Supplementary Material to this article). Here, we adopt the results from Hu et al. (2022) and incorporate an LVT with a tapering depth of 1000 m at sites outside the basin area in the WFCVM. The LVT reduces the surface V_s values outside the Salt Lake basin from about 1400 m/s in the WFCVM to about 800 m/s, see Figures S2 and S3.

To constrain the anelastic attenuation parameters of the Salt Lake basin, we tested models with a range of frequency-dependent Q parameter combinations (Equation 1) where $Q_S/V_S =$ [0.05 – 0.1] and $\gamma =$ [0.3 – 0.6]. In these simulations, an attenuation model with $Q_S = 0.05V_S$ for frequencies less than 1 Hz and $Q_S = 0.05V_S f^{0.4}$ for frequencies higher than 1 Hz (V_s in m/s) provided the smallest FAS bias, as shown in Figure 3, at stations within a distance of 30 km to the epicenter.

SSHs

The synthetics generated in the reference WFCVM show a notable underprediction in coda waves in the synthetics (see Figure S4), and we tested whether distributions of SSHs blended into the top 1 km of the WFCVM are able to improve this deficiency. Specifically, we tested SSHs with a von Kármán auto-correlation function model and vertical correlation lengths (Lz) between 80 and 400 m, horizontal-to-vertical anisotropy of 5, and standard deviations with respect to the background WFCVM velocities and densities $\sigma = [5 - 10]\%$, as derived from boreholes in the Los Angeles basin by Savran and Olsen (2016). Our results show that a model with $Lz = 400$ m, $\sigma = 10\%$, and a Hurst number of 0.05 considerably improves the duration of the later arrivals (see Figure S5), and also

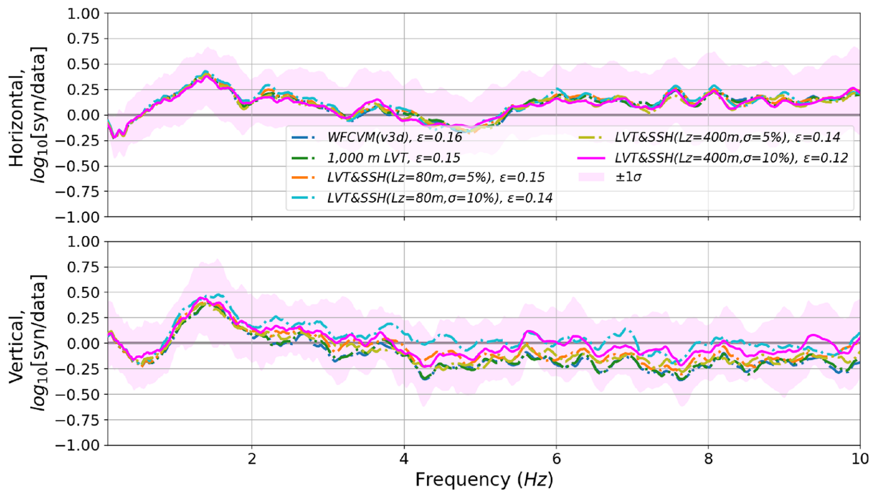

Figure 4. Same as Figure 3, but for tests with different vertical correlation lengths (Lz) and standard deviations (σ) of SSHs. All results include an LVT with 1000 m tapering depth outside the basins and the optimal Q model. The magenta curve is derived from the optimal choice of SSH parameters.

provides the smallest FAS bias to observations (Figure 4). Figure S3 compares the surface V_s values for the WFCVM before and after adding the LVT and SSHs, illustrating the added complexity in the latter model.

Simulations versus observations

Comparisons between waveforms and Fourier spectra from seismic records and optimal synthetics within the model domain are shown in Figure 5 for the bandwidth 0.1–1.0 Hz, and Figure S4 provides similar comparisons for 0.1–10.0 Hz. Figures 6 and 7 show the GOF for our four selected metrics for bandwidths of 0.1–1.0 Hz and 0.1–10 Hz, respectively. The simulations track the seismic records reasonably well in arrival times, Fourier Spectra, waveforms of the main phases, as well as durations for the low frequencies. The 0.1–1.0 Hz GOF values generally fall within the "fair" (45–65) and "very good" (65–80) rating by Olsen and Mayhew, with a few stations obtaining "excellent" (80–100) ratings. However, as expected, the waveform fit is significantly degraded as the higher frequencies are included, as the effects from largely unconstrained small-scale complexities in the velocity model increase. For the low frequency band, the simulations tend to underpredict the ground motions at stations located near the epicenter (e.g. VEC, LKC, ICF, FTT, and SCC), and overpredict at stations further to the east, near the basin edge (e.g. AVE, UUE, and WES) for both low and high frequencies. These discrepancies likely reflect inaccuracies in the WFCVM (see "Discussion" section).

Finite-fault models for the 2020 Magna mainshock

Using the WFCVM with our calibrated model parameters, we proceed to simulations of the 2020 Magna mainshock. First, we evaluate seven different finite-fault source descriptions, namely, six models obtained from the Graves-Pitarka (GP) kinematic rupture generator (Graves and Pitarka, 2010, 2015; Pitarka et al., 2021), as well as the kinematic model inverted by Pollitz et al. (2021), see Table 3(g). The source descriptions from the

GP rupture generator incorporate randomized spatial heterogeneity in slip, rupture speed, rise time, and rake angle optimized against strong-motion recordings, and have been shown to generate realistic finite-fault source models for frequencies up to 5–10 Hz (e.g. Hu et al., 2022; Rodgers et al., 2020). For all the tested GP source descriptions, we applied

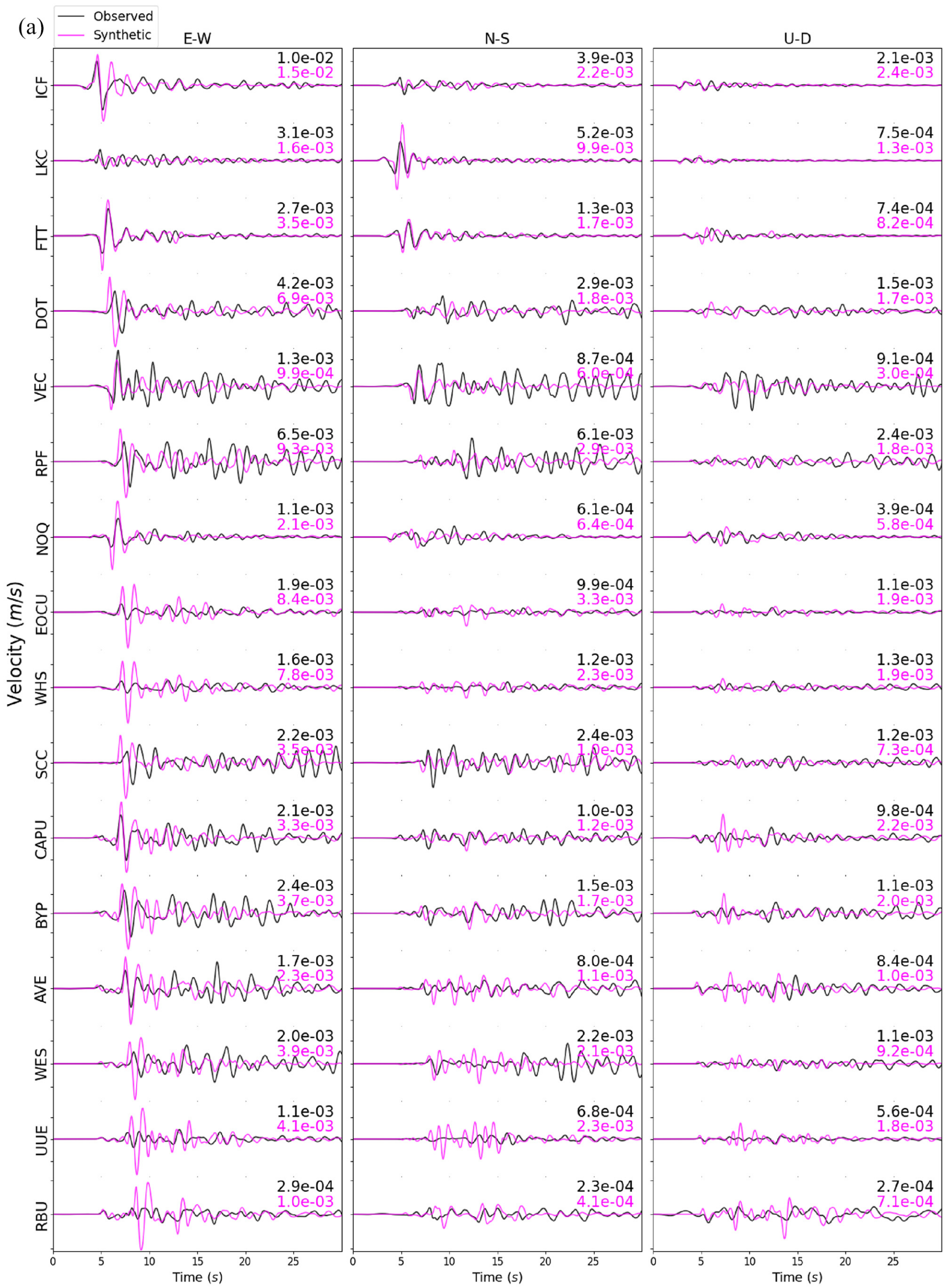

Figure 5. Continued.

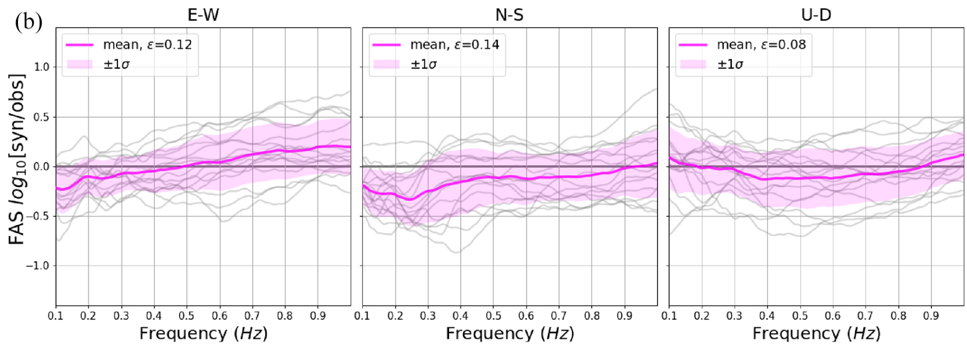

Figure 5. Comparison of 0.1–1.0 Hz synthetics from our optimal model and observations for the M_w4.59 aftershock. (a) Velocity time series, with peak values for both synthetic and observed listed in m/s, and (b) Fourier acceleration spectral bias, with ε depicting mean error over all stations. See Figure 1b for station locations.

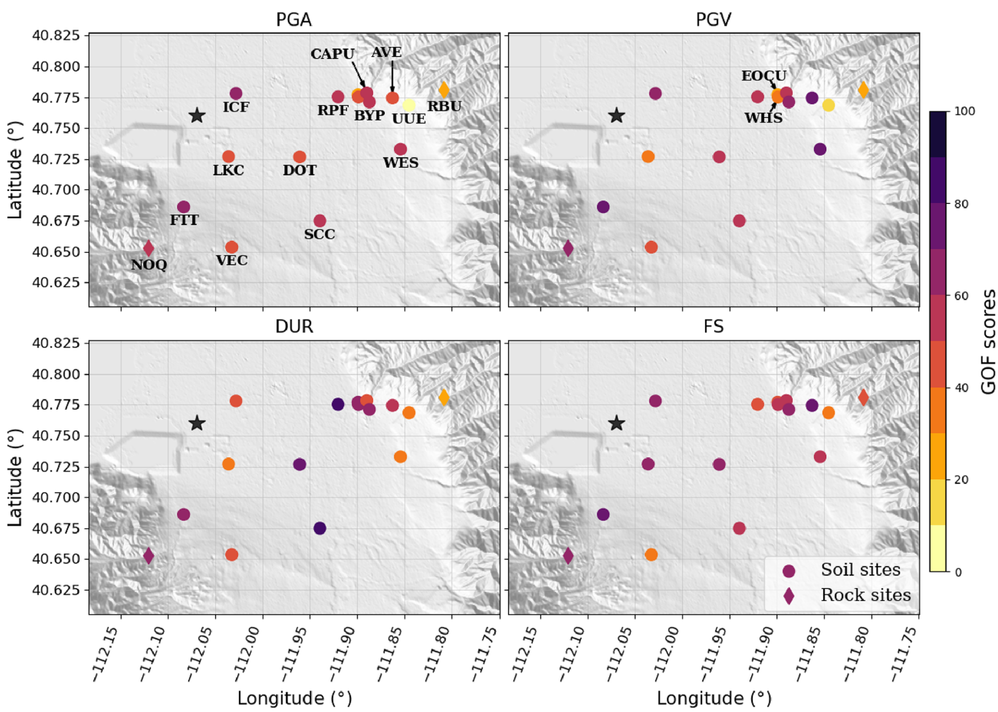

Figure 6. GOF maps for 0.1–1.0 Hz PGA, PGV, DUR, and FS from our optimal linear simulation of the M_w4.59 aftershock. The epicenter is denoted by the star.

the moment tensor solution from Pang et al. (2020) with magnitude-fault area relations including the Leonard (2010) mean relation model and $\pm 1\sigma$ (4500–5860 m), as well as a range of fault lengths along strike for a M_w5.5 event from Wells and Coppersmith (1994) (2180–7790 m), see Table 3. Note that the six GP-generated sources include realizations of different slip and rupture time distributions (Figure 8).

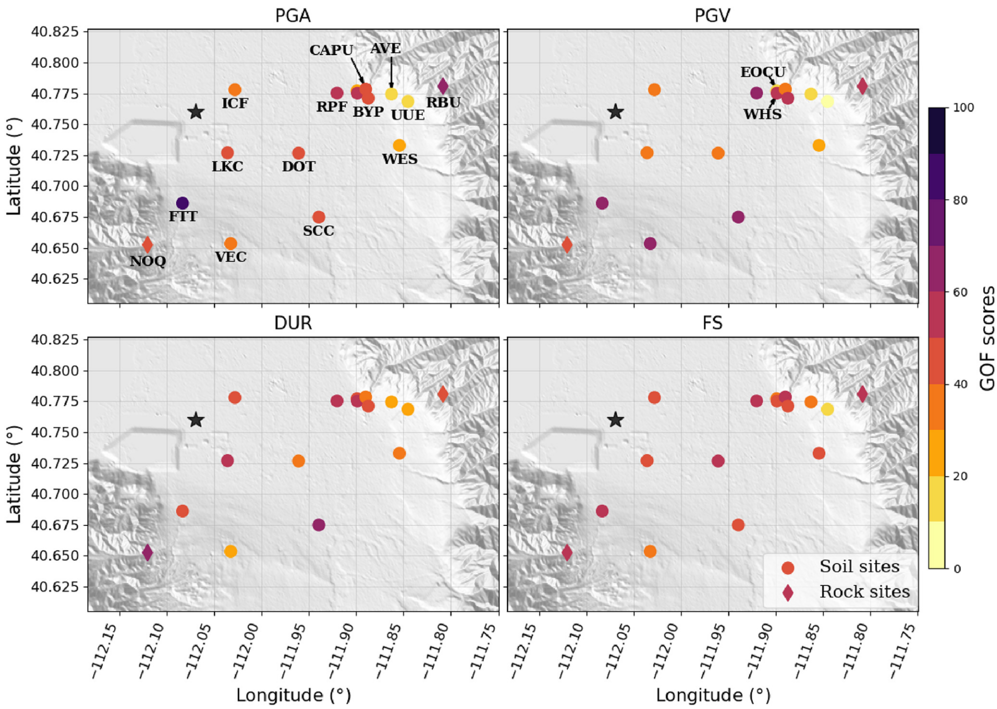

Figure 7. Same as Figure 6, but for synthetics and data band-pass filtered between 0.1 and 10.0 Hz.

Table 3. Kinematic finite-fault models of the Magna mainshock used in this project, all with a hypocentral location of (40.7521°N, 112.0575°W), strike/dip/rake of 182°/34°/.52° and a moment magnitude of M_w 5.54 (from Pang et al., 2020) for all models. Slip and rupture time distributions are shown in Figure 8

Model #	Hypocentral depth (m)	Length (m)	Width (m)	Description
(a)	9000	5860	4400	mean model (Leonard, 2010)
(b)	9000	8450	4560	$+1\sigma$ model (Leonard, 2010)
(c)	9000	4500	3000	-1σ model (Leonard, 2010)
(d)	9000	7790	6310	mean model (Wells and Coppersmith, 1994)
(e)	9000	2180	1830	$a-1\sigma$, $b-1\sigma$ model (a, b in Table 2A, Wells and Coppersmith, 1994)
(f)	8000	3620	3330	$b-1\sigma$ model (b in Table 2A, Wells and Coppersmith, 1994)
(g)	8000	10,000	16,100	kinematic source inversion (Pollitz et al., 2021)

Figure 9 shows FAS comparisons of our simulations for different Magna mainshock source models in the linear regime to the seismic records for frequencies 0.1–1.0 Hz, where nonlinear soil effects are largely absent, and 0.1–10 Hz. All the tested source models generally underpredict the data at the low frequencies, the kinematic inversion model most significantly by over 70%. A primary reason for the underprediction observed for the

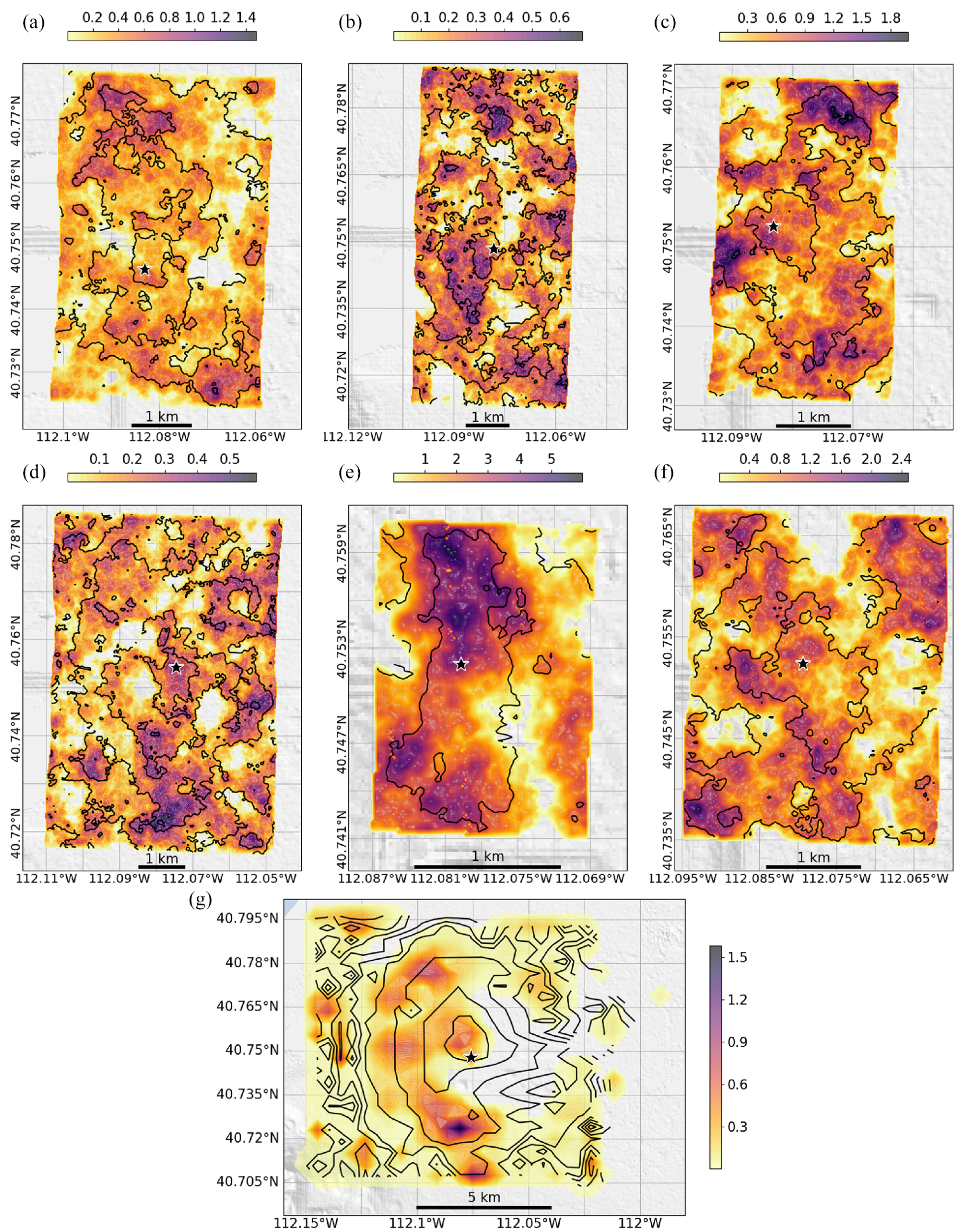

Figure 8. Candidate source models (a–g) tested for the Magna mainshock with locations shown (see Figure 1b for location—note differences in fault size). The slip distribution (in meters) is depicted by color shading, rupture times by contours with 0.4 s intervals, and the hypocenter by a star. Models (a–f) are generated from the GP rupture generator (Pitarka et al., 2021), while model (g) is the finite-fault slip model from the kinematic coseismic slip inversion by Pollitz et al. (2021) (see also Table 3). The background gray shading depicts topography. Model (f) is selected for all nonlinear simulations.

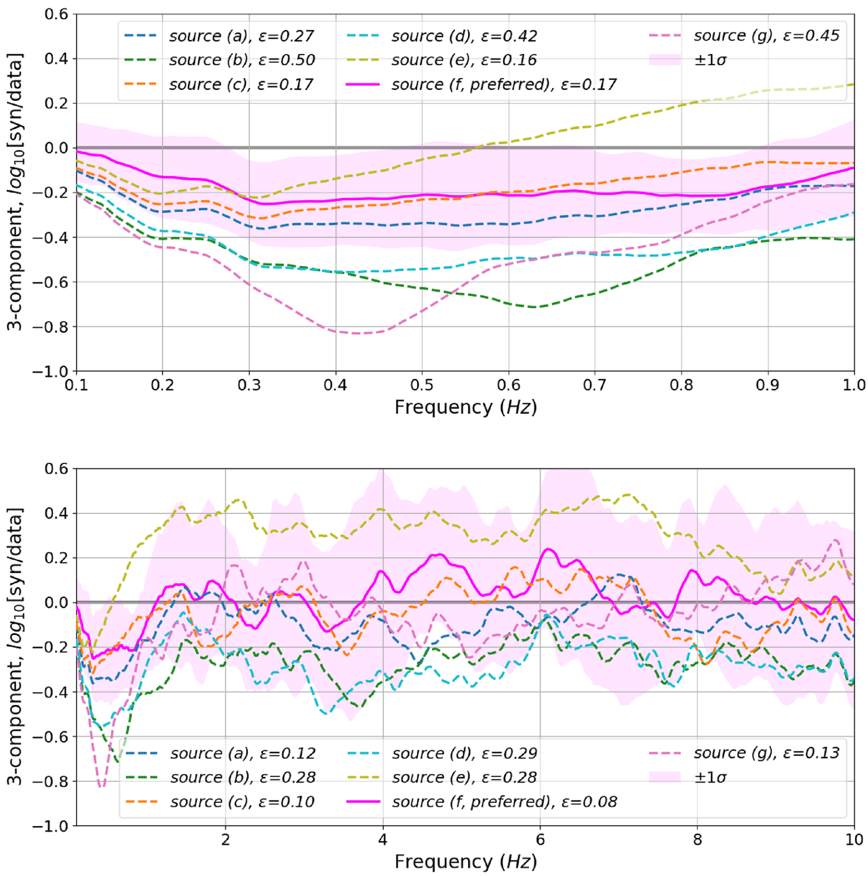

Figure 9. Comparison between FAS bias derived from the seven finite-fault models of the Magna mainshock (averaged over 16 stations), simulated in the linear regime and band-pass filtered between 0.1 and 1.0 Hz in the top panel and 0.1–10.0 Hz in the bottom panel, using the optimal velocity model from the validations shown in Figure 4. The color shading shows the $\pm 1\sigma$ range of the preferred model, and the three-component averaged absolute error values (ε, in log scale) are listed in the legend for each source model.

inverted source is likely the low-pass filtering applied at a corner frequency of 0.25 Hz for the seismic recordings in Pollitz et al. (2021), that is, the inversion results are deficient in seismic energy at frequencies higher than about 0.25 Hz. The general underprediction of the low-frequency FAS from the mainshock models is likely caused by inaccuracies in the WFCVM, as a similar pattern was found for the M_w4.59 aftershock (see Figure 4). Our preferred rupture model (Figure 9f), which provides a near-constant bias of about –0.2 in log10 units, uses a 3600 m by 3300 m fault plane extending from a depth of 7100 m to 8900 m (hypocentral depth of 8000 m), following the -1σ relations in Wells and Coppersmith (1994) Table 3 and Figure 8. For the bandwidth 0.1–10 Hz, our preferred source model generates the smallest bias to the recordings from the Magna mainshock. The largest (smallest) fault sizes generate bias values near -1σ ($+1\sigma$) for our preferred model.

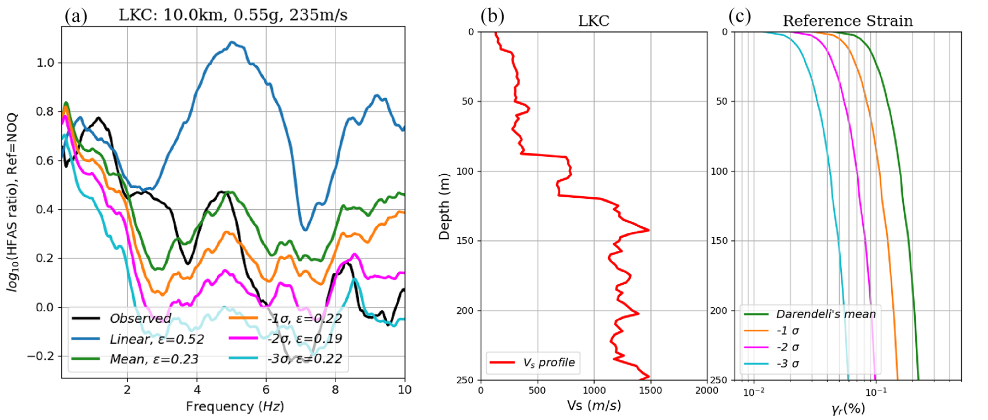

Figure 10. (a) Comparison of synthetic and observed spectral amplification ratios for the Magna mainshock at near-fault soil station LKC, comparing linear results to nonlinear simulations using Darendeli's reference strain–depth relation mean values (green) as well as -1σ, -2σ, and -3σ relations. The spectral ratios all use NOQ as a reference station. (b) V_s profile from the WFCVM, modified with SSHs at LKC. (c) Corresponding reference strain–depth relations based on the velocity model, using the same color specifications as in the left panel.

Calibration of nonlinear rheology parameters

To constrain the nonlinear properties, we use the three stations that recorded the largest PGAs and represent the smallest epicentral distances to the mainshock epicenter, namely, LKC (9.2 km, PGA 0.55 *g*), ICF (9.5 km, PGA 0.34 *g*), and FTT (10.8 km, PGA 0.40 *g*), see Figure 1b for locations. The controlling parameter in the multi-yield surface nonlinear model is the reference strain γ_r. We first test the empirical relations of reference strain versus depth by Darendeli (2001), which corresponds to several in situ and laboratory observations from the Salt Lake Valley. Nonlinear effects are constrained to the shallow unconsolidated sediments by increasing γ_r in the underlying consolidated sediments and bedrock to a very large value (1.0), and we specify this transition where V_s increases above 2,000 m/s (see Roten et al., 2012). However, the effects of moving this threshold to a shallower depth are relatively small, see Figure S8 in the Supplementary Material.

Roten et al. (2023) showed that the multi-surface Iwan method converges for 7 to 10 yield surfaces. As significant additional computational requirements are needed for an increasing number of yield surfaces, we test the accuracy of using 7 and 10 yield surfaces at LKC (Figure S8). As only a minor increase in accuracy is obtained from 7 to 10 yield surfaces, we use seven yield surfaces in our nonlinear simulations to save computational resources.

Due to the underprediction in the epicentral area of the observed seismic records at ICF, LKC, and FTT for the aftershock simulation, and in general for the finite-fault sources at lower frequencies (see Figure 6 and Figure S6 in the supplementary material), we use spectral ratios to calibrate the nonlinear parameters which, calculated with an appropriate reference 'rock' site, have the potential to minimize source effects or a bias in the WFCVM structure (see Pankow and Pechmann, 2004, Equation S14 and the Supplementary Material to this article for details in the spectral ratio calculation). Here, we use records and synthetics at station NOQ in the nearby Oquirrh Mts, just southwest

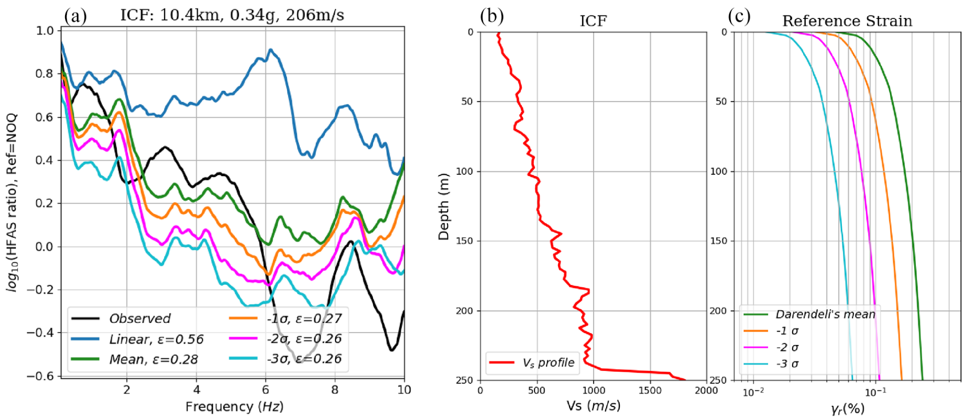

Figure 11. Same as Figure 10, but for station ICF.

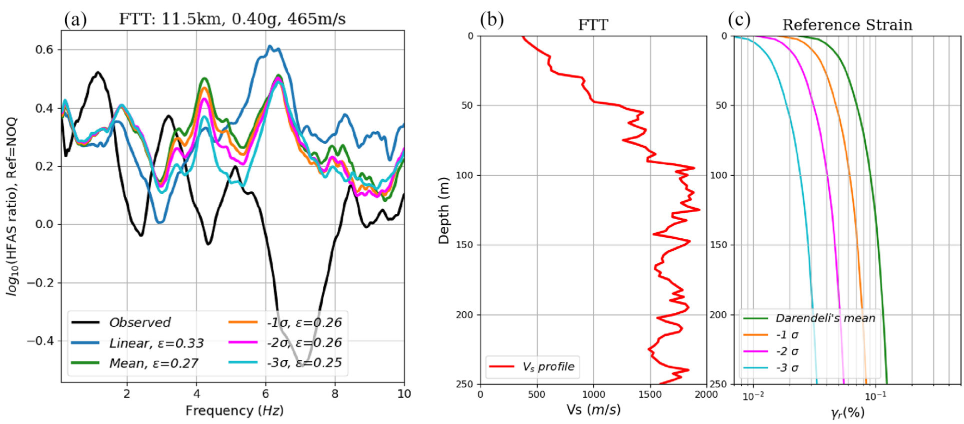

Figure 12. Same as Figure 10, but for station FTT.

of ICF, LKC, and FTT. The spectral ratios using the simulation in the linear regime generally overpredict the observed records at the three stations, as expected in the presence of nonlinear effects.

When applying the Iwan-type nonlinear modeling method with seven yield surfaces and the mean reference strain relations from Darendeli (2001) (Figure 10), nonlinear damping reduces the modeled spectral ratios at the higher frequencies by factors of up to 6 for all three stations to a level much closer to those for those for the observations (Figures 10 to 12). This result further suggests that the epicentral area was significantly affected by nonlinear effects during the 2020 Magna mainshock.

Considering that in situ and laboratory observations for nonlinear soil properties are sparse in the Salt Lake Basin, and the local reference strains at shallow depths (<150 m) have a high variance (Bay and Sasanakul, 2005), we also tested Darendeli's reference strain model at –1, –2, and –3 standard deviations (σ). While further damping the high-frequency ground motions, the added reduction in FAS from the mean relation to the –1, –2, and –3

σ relations is considerably smaller than that obtained from the mean relation itself. We find that reference strains at Darendeli's -2σ relation result in the smallest bias at all three stations using spectral ratios (Figures 10 to 12). However, while this reference strain model is able to bring the modeled spectral accelerations into much improved agreement with those from the seismic recordings at LKC and ICF, the damping of the high-frequency spectral energy and improvement at station FTT is limited (Figure 12). The reason for the inability of the nonlinear model to generate improved synthetics at FTT is likely related to the thinner low-velocity sediments at this site (around 30 m, see Figure 12b and c). The need for reference strains smaller than the Darendeli mean relations to provide an optimal fit to the data may be attributed to the relatively thin but softer soils in the Magna area, close to the western boundary of the Salt Lake basin, while the Darendeli mean relations were obtained for samples in deeper parts of the basin. In addition, uncertainty of the mainshock source model used in the simulations may be a contributing factor in the smaller-than-expected reference strains (see "Discussion" section).

Discussion

For simulations of both the mainshock and the M_w4.59 aftershock of the 2020 Magna sequence, we adopted the source locations and moment tensor solutions provided by Pang et al. (2020) and University of Utah (2020b) ("UUSS model"). However, it is important to consider the uncertainty introduced by the simple velocity model used to determine the location and focal mechanism of the events (five-layer Western US one-dimensional (1D) model following Herrmann et al. (2011)), as well as the relatively low-frequency data used (low-pass filtered below 10 s). From variance reduction and residual-depth relations by Pang et al. (2020), the uncertainty of the centroid depth for the aftershock is about 2000 m. Similarly, the moment tensor solution given by Saint Louis University (2020), which is restricted to a double-couple source model, provides a difference in seismic moment and depth of around 15% compared to the UUSS model.

However, uncertainty in the source depth will not resolve the problem of simultaneous underprediction in the epicentral area and overprediction near the eastern edge of the WFCVM. The overestimation of the synthetic ground motions against the observations at basin-edge stations which can exceed a factor-of-two, such as at AVE and UUE in Figure S4(a), may be caused by lower impedance and a deeper depth to the bottom of the Salt Lake basin than currently included in the WFCVM. In addition, a more realistic geometry of the basin along its edges, where the sediments at many sites are less than 50 m thick, may improve the fit between synthetics and data. The WFCVM is likely better constrained near downtown Salt Lake City, with a larger quantity of well data providing borehole information, as well as subsurface geometry of the Wasatch fault (Pechmann et al., 2022). Moreover, Hutchings (2023) suggests from numerical simulations of the Magna mainshock that the eastern part of the basin structure, between the Wasatch Fault and the West Valley Fault Zone, is not well constrained in the WFCVM. Furthermore, the study proposes that a deeper basin bottom than what is included in the WFCVM as the "sediment-bedrock interfaces" (R3) by Magistrale et al. (2008) is needed to increase the basin amplification in the eastern Salt Lake basin. We recommend further work to constrain the velocity structure of the Salt Lake basin sediments and surrounding area.

The accuracy of the reference strain values estimated for the Salt Lake basin near the epicentral area of the 2020 Magna mainshock in this study depends on whether our preferred finite-fault source description, with a fault area one standard deviation below that

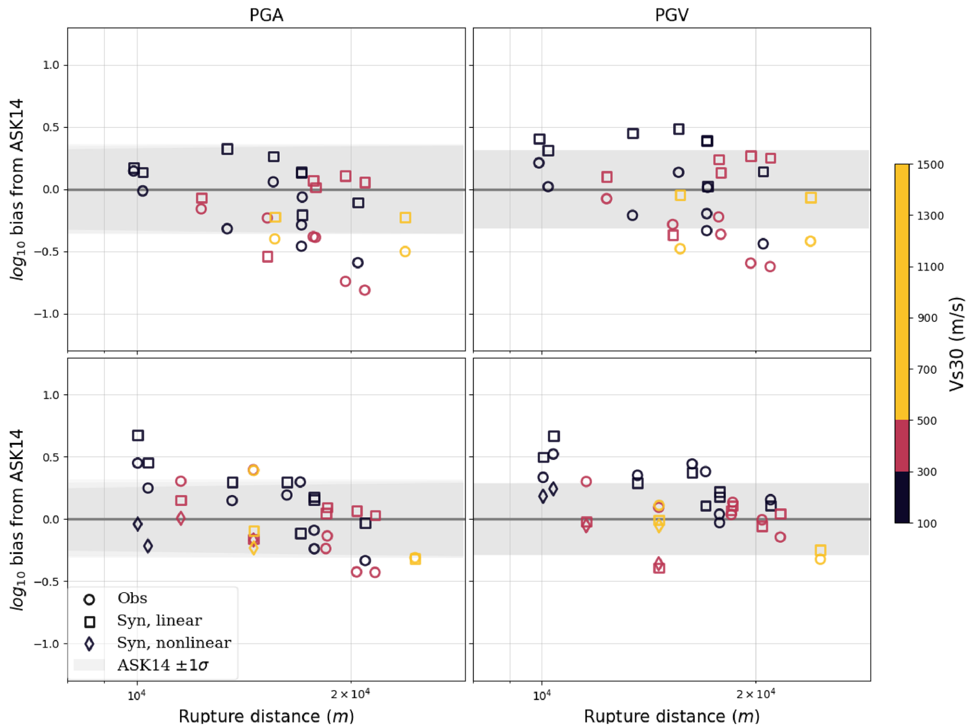

Figure 13. Comparison of bias for PGA (left column) and PGV (right column), from (top row) the M_w4.59 aftershock, and (bottom row) the Magna main shock, relative to ASK14. Stations are divided into three V_{s30} bins: 100–300 m/s, 300–500 m/s, and >500 m/s.

from the mean magnitude-area by Wells and Coppersmith (1994), generates a realistic level of high-frequency ground motions. Larger fault areas (i.e. near or larger than those dictated by the mean relations by Wells and Coppersmith (1994) and Leonard (2010)) would likely generate lower peak motions in the linear regime, and thus demand larger reference strains and smaller nonlinear damping. Future work should conduct nonlinear simulations for additional finite-fault solutions of the Magna mainshock to further constrain the reference strains in the epicentral area. These simulations should include stations in the Salt Lake basin to the east of our nonlinear modeling domain, omitted in this study due to computational demands, to further test the presumed threshold for nonlinear soil effects at about 0.1 g.

Figure S9 shows the minimum value of the shear modulus G, normalized by the low-strain shear modulus G_{max}, at the surface of the domain for the case of Darendeli's (2001) reference strain–depth relation minus 2σ. With a grid spacing of $\Delta h = 2.5$ m, the simulations resolve frequencies up to 10 Hz with more than five points per minimum wavelength in the linear regime at all sites. However, because of the shear modulus degradation, the effective V_s and therefore the frequency limit are reduced in the nonlinear simulations. At LKC, the minimum shear modulus is reduced to 0.09 times its undamped value, resulting in a surface V_s of 43 m/s during the nonlinear damping. To test whether a grid spacing smaller than $\Delta h = 2.5$ m is needed to resolve the nonlinear ground motions, we conducted two-dimensional (2D) simulations using a two-step method, allowing for a smaller grid spacing that resolves the reduced V_s in the near-surface material ($\Delta h = 0.85$ m) by at least five points per wavelength. The results (see Figures S10 and S11 and associated discussion in the Supplemental Material) suggest that the 3D simulations accurately resolve the non-linear damping in our 3D simulations.

Topography was not included in our simulations, and the omission may have biased the results somewhat. However, we expect such bias to be small, due to the location of the Magna sequence directly below the Salt Lake Valley, likely generating very limited topographic scattering. In any case, we recommend that the effects of topography on ground motions in the Salt Lake Valley be investigated in future work.

Finally, GMMs can be useful tools to predict ground motion measures, and the seismic recordings from the Magna earthquake series provide an excellent opportunity to test their accuracy. Figure 13 shows residuals to the NGA-West2 ASK14 GMM (Abrahamson et al., 2014) from both observations and our simulations for the M_w4.59 Magna aftershock and mainshock for both PGAs and PGVs. For the Magna mainshock, both the GMM (as also pointed out by Wong et al., 2021) and the simulation generally predict the recorded PGA values within one standard deviation, while the GMM slightly underpredicts the PGVs from both observations and synthetics, most notably for the lowest Vs_{30} values (200 $\pm$. 50 m/s). The nonlinear damping brings the PGAs and PGVs for the simulations closer to agreement with the GMM. For the aftershock, both the GMM and synthetics slightly overpredict the observed PGAs and PGVs.

Conclusions

We have carried out 0–10 Hz 3D wave propagation simulations of the 2020 Magna mainshock and a M_w4.59 aftershock in the WFCVM. Comparison of our simulations of the aftershock in the linear regime to seismic recordings shows that frequency-dependent anelastic attenuation as $Q_s = 0.05V_s$ (f <1 Hz) and $Q_s(f) = 0.05V_s f^{0.4}$ (f >1 Hz, V_s in m/s), along with a von Kármán distribution of small-scale velocity heterogeneities with 10% standard deviation in the top 1 km of the model generate an optimal fit. However, our simulations generally underpredict the seismic data at stations located near the epicenter and overpredict the seismic records at sites at the eastern edge of the Salt Lake basin, likely due to inaccuracies in the velocity structure of the WFCVM. Spectral rations from our simulations with our preferred finite-fault realization of the source of the 2020 Magna mainshock in the linear regime tend to overestimate the high-frequency seismic records at stations near the epicenter. Using a fully hysteretic multi-yield-surface 3D nonlinear modeling approach (Roten et al., 2023), we find that the reference strain–depth relations proposed by Darendeli (2001) provide damping that significantly improves the fit between simulated and recorded 0–10 Hz spectral ratios at stations with the largest PGA values (LKC, 0.55 *g*, ICF, 0.34 *g*, and FTT, 0.40 *g*). We find an optimal fit between the high-frequency spectral ratios for the recordings and nonlinear synthetics at these stations for reference strains of 2 standard deviations below those proposed by Darendeli (2001), reducing the bias by more than a factor of two. Our constraints on the nonlinear properties in the Salt Lake Valley provide a basis for improved seismic hazard analyses of the greater Salt Lake City region.

Acknowledgments

We thank Jim Pechmann and three anonymous reviewers for valuable comments and suggestions.

Declaration of conflicting interests

The author(s) declared no potential conflicts of interest with respect to the research, authorship, and/or publication of this article.

Funding

The author(s) disclosed receipt of the following financial support for the research, authorship, and/or publication of this article: The research was supported by the U.S. Geological Survey (USGS), Department of the Interior, under USGS award number G22AP00033. The views and conclusions contained in this document are those of the authors and should not be interpreted as necessarily representing the official policies, either expressed or implied, of the U.S. Government.

ORCID iDs

Ke Xu https://orcid.org/0000-0002-6991-1158
Te-Yang Yeh https://orcid.org/0000-0002-9146-6804

Data and resources

The ground motion data used in this project were downloaded from the Incorporated Research Institutions for Seismology (IRIS) web service via the ObsPy client (https://docs.obspy.org/packages/obspy.clients.fdsn.html). All simulated time series can be downloaded from the Zenodo repository by Xu and Olsen (2024). The Wasatch Front Community Velocity Model (WFCVM) version 3d is available from the Utah Geological Survey (https://geology.utah.gov/hazards/assistance/consultants/cvm-geophysical/). This research used resources of the Oak Ridge Leadership Computing Facility at the Oak Ridge National Laboratory, which is supported by the Office of Science of the US Department of Energy under Contract No. DE-AC05-00OR22725.

Most of the data-processing work was done using Python and the Generic Mapping Tools package (https://www.generic-mapping-tools.org, last accessed June 2024). Configuration parameters, input files, and synthetic IMs for this work are available at https://doi.org/10.5281/zenodo.10892429. AWP-ODC is open source and freely available at https://github.com/HPGeoC/awp-odc-os.

Supplemental material

Supplemental material for this article is available online.

References

Abrahamson NA, Silva WJ and Kamai R (2014) Summary of the ASK14 ground motion relation for active crustal regions. *Earthquake Spectra* 30: 1025–1055.

Bay JA and Sasanakul I (2005) *Measurement of Nonlinear Dynamic Properties of Bonneville Silty-Clays: NIW Program*. Logan, UT: Department of Civil and Environmental Engineering, Utah State University.

Beresnev IA and Wen K-L (1996) Nonlinear soil response—A reality? *Bulletin of the Seismological Society of America* 86: 1964–1978.

Black BD, Lund WR and Mayes BH (1995) Large Earthquakes on the Salt Lake City segment of the Wasatch Fault Zone–Summary of new information from the South Fork Dry Creek Site, Salt Lake County, Utah. *Utah Geological Association Publication* 24: 11–30.

Brocher TM (2008) Key elements of regional seismic velocity models for long period ground motion simulations. *Journal of Seismology* 12: 217–221.

Brune JN (1970) Tectonic stress and the spectra of seismic shear waves from earthquakes. *Journal of Geophysical Research* 75: 4997–5009.

Cui Y, Poyraz E, Olsen KB, Zhou J, Withers K, Callaghan S, Larkin J, Guest C, Choi D, Chourasia A, Shi Z, Day SM, Maechling PJ and Jordan TH (2013) Physics-based seismic hazard analysis on petascale heterogeneous supercomputers. In: *Proceedings of the international conference on high performance computing, networking, storage and analysis*, Denver, CO, 17–22 November, pp. 1–12. New York: IEEE.

Darendeli MB (2001) *Development of a new family of normalized modulus reduction and material damping curves*. PhD Thesis, The University of Texas at Austin, Austin, TX.

DuRoss CB (2008) Holocene vertical displacement on the central segments of the Wasatch Fault Zone, Utah. *Bulletin of the Seismological Society of America* 98: 2918–2933.

DuRoss CB, Personius SF, Crone AJ, Olig SS, Hylland MD, Lund WR and Schwartz DP (2016) Fault segmentation: New concepts from the Wasatch Fault Zone, Utah, USA. *Journal of Geophysical Research: Solid Earth* 121: 1131–1157.

Ely G, Jordan T, Small P and Maechling P (2010) A Vs30-derived near-surface seismic velocity model. *AGU Fall Meeting Abstracts* 2010: S51A–S1907.

Gottschämmer E and Olsen KB (2001) Accuracy of the explicit planar free-surface boundary condition implemented in a fourth-order staggered-grid velocity-stress finite-difference scheme. *Bulletin of the Seismological Society of America* 91: 617–623.

Graves R and Pitarka A (2010) Broadband ground-motion simulation using a hybrid approach. *Bulletin of the Seismological Society of America* 100: 29.

Graves R and Pitarka A (2015) Refinements to the Graves and Pitarka (2010) broadband ground-motion simulation method. *Seismological Research Letters* 86: 75–80.

Herrmann RB, Benz H and Ammon CJ (2011) Monitoring the earthquake source process in North America. *Bulletin of the Seismological Society of America* 101: 2609–2625.

Hu Z, Olsen KB and Day SM (2022) 0–5 Hz deterministic 3-D ground motion simulations for the 2014 La Habra, California, Earthquake. *Geophysical Journal International* 230: 2162–2182.

Hutchings SJ (2023) *Simulation of high frequency ground motion for the 18 March 2020 Mw 5.7 Magna, Utah, earthquake using the Wasatch Front Community Velocity Model (WFCVM)*. PhD thesis, ProQuest Dissertations Publishing.

Iwan WD (1967) On a class of models for the yielding behavior of continuous and composite systems. *Journal of Applied Mechanics* 34: 612–617.

Jaiswal K, Rozelle J and Bausch D (2023) *Hazus® estimated annualized earthquake losses for the United States*. Technical report FEMA P-366, Washington, DC: Federal Emergency Management Agency.

Kaklamanos J, Bradley BA, Thompson EM and Baise LG (2013) Critical parameters affecting bias and variability in site-response analyses using KiK-net Downhole array data. *Bulletin of the Seismological Society of America* 103: 1733–1749.

Kaklamanos J, Dorfmann L and Baise LG (2015) A simple approach to site-response modeling: The overlay concept. *Seismological Research Letters* 86: 413–423.

Kleber EJ, McKean AP, Hiscock AI, Hylland MD, Hardwick CL, McDonald GN, Anderson ZW, Bowman SD, Willis GC and Erickson BA (2020) Geologic setting, ground effects, and proposed structural model for the 18 March 2020 Mw 5.7 Magna, Utah, earthquake. *Seismological Research Letters* 92: 710–724.

Leonard M (2010) Earthquake fault scaling: Self-consistent relating of rupture length, width, average displacement, and moment release. *Bulletin of the Seismological Society of America* 100: 1971–1988.

McCalpin J and Nelson C (2000) *Long Recurrence Records from the Wasatch Fault Zone*. Technical report 99HQGR0058. Salt Lake City, UT: National Earthquake Hazards Reduction Program, U.S. Geological Survey.

McCalpin JP and Nishenko SP (1996) Holocene paleoseismicity, temporal clustering, and probabilities of future large ($M > 7$) earthquakes on the Wasatch fault zone, Utah. *Journal of Geophysical Research: Solid Earth* 101: 6233–6253.

Machette MN, Personius SF and Nelson AR (1992) *Paleoseismology of the Wasatch Fault Zone: A summary of recent investigations, interpretations, and conclusions*. Technical report 1500-A. Reston, VA: U.S. Geological Survey.

Machette MN, Personius SF, Nelson AR, Schwartz DP and Lund WR (1991) The Wasatch fault zone, Utah—segmentation and history of Holocene earthquakes. *Journal of Structural Geology* 13: 137–149.

Magistrale H, Pechmann JC and Olsen KB (2008) *Construction and verification of a Wasatch Front Community Velocity Model*. Technical report HQGR.060012. Reston, VA: U.S. Geological Survey.

Masing G (1926) Eigenspannumyen und verfeshungung beim messing. In: *Proceedings of the international congress for applied mechanics*, Zurich, 12-17 September 1926, pp. 332–335.

Moschetti MP, Hartzell S, Ramírez-Guzmán L, Frankel AD, Angster SJ and Stephenson WJ (2017) ⩾ 3D ground-motion simulations of M w 7 earthquakes on the Salt Lake City segment of the Wasatch fault zone: Variability of long-period (T ⩾ 1 s) ground motions and sensitivity to kinematic rupture parameters. *Bulletin of the Seismological Society of America* 107: 1704–1723.

Mróz Z (1967) On the description of anisotropic work hardening. *Journal of the Mechanics and Physics of Solids* 15: 163–175.

Nie S, Wang Y, Olsen KB and Day SM (2017) Fourth-order staggered-grid finite-difference seismic wavefield estimation using a discontinuous mesh interface (WEDMI). *Bulletin of the Seismological Society of America* 107: 2183–2193.

Olsen KB and Mayhew JE (2010) Goodness-of-fit criteria for broadband synthetic seismograms, with application to the 2008 Mw 5.4 Chino Hills, California, Earthquake. *Seismological Research Letters* 81: 715–723.

Pang G, Koper KD, Mesimeri M, Pankow KL, Baker B, Farrell J, Holt J, Hale JM, Roberson P, Burlacu R, Pechmann JC, Whidden K, Holt MM, Allam A and DuRoss C (2020) Seismic analysis of the 2020 Magna, Utah, earthquake sequence: Evidence for a Listric Wasatch Fault. *Geophysical Research Letters* 47: e2020GL089798.

Pankow KL and Pechmann JC (2004) *Determination of Low-strain Site-amplification Factors in the Salt Lake Valley, Utah, Using ANSS Data*. Salt Lake City, UT: University of Utah Seismograph Stations.

Pankow KL, Rusho J, Pechmann JC, Hale JM, Whidden K, Sumsion R, Holt J, Mesimeri M, Wells D and Koper KD (2020) Responding to the 2020 Magna, Utah, earthquake sequence during the COVID-19 pandemic shutdown. *Seismological Research Letters* 92: 6–16.

Parker GA, Moschetti MP and Thompson EM (2023) Ground-motion variability from kinematic rupture models and the implications for nonergodic probabilistic seismic hazard analysis. *Seismological Research Letters* 94: 2687–2697.

Pechmann J, Wong I, DuRoss C, Hylland M, Crone A, Personius S, McKean A, Arabasz W, Schwartz D, Olig S, Lund W and Dinter D (2022) A logic tree for the subsurface geometry of the Salt Lake City segment of the Wasatch fault in light of the 2020 Magna, Utah, earthquake. In: *Proceedings volume 2022 basin and range earthquake summit*, Salt Lake City, UT, 17–20 October.

Pitarka A, Graves R, Irikura K, Miyakoshi K, Wu C, Kawase H, Rodgers A and McCallen D (2021) Refinements to the Graves–Pitarka kinematic rupture generator, including a dynamically consistent slip-rate function, applied to the 2019 Mw 7.1 ridgecrest earthquake. *Bulletin of the Seismological Society of America* 112: 287–306.

Pollitz FF, Wicks CW and Svarc JL (2021) Coseismic fault slip and afterslip associated with the 18 March 2020 M 5.7 Magna, Utah, earthquake. *Seismological Research Letters* 92: 741–754.

Rajaure S, Asimaki D, Thompson EM, Hough S, Martin S, Ampuero JP, Dhital MR, Inbal A, Takai N, Shigefuji M, Bijukchhen S, Ichiyanagi M, Sasatani T and Paudel L (2017) Characterizing the Kathmandu Valley sediment response through strong motion recordings of the 2015 Gorkha earthquake sequence. *Tectonophysics* 714–715: 146–157.

Rodgers AJ, Pitarka A, Pankajakshan R, Sjögreen B and Petersson NA (2020) Regional-scale 3D ground-motion simulations of Mw 7 earthquakes on the Hayward Fault, Northern California resolving frequencies 0–10 Hz and including site-response corrections. *Bulletin of the Seismological Society of America* 110: 2862–2881.

Roten D, Olsen KB and Pechmann JC (2012) 3D simulations of M 7 earthquakes on the Wasatch Fault, Utah, Part II: broadband (0–10 Hz) ground motions and nonlinear soil behavior. *Bulletin of the Seismological Society of America* 102: 2008–2030.

Roten D, Olsen KB, Pechmann JC, Cruz-Atienza VM and Magistrale H (2011) 3D simulations of M 7 earthquakes on the Wasatch Fault, Utah, Part I: Long-period (0–1 Hz) ground motion. *Bulletin of the Seismological Society of America* 101: 2045–2063.

Roten D, Yeh T, Olsen KB, Day SM and Cui Y (2023) Implementation of Iwan-type nonlinear rheology in a 3D high-order staggered-grid finite-difference method. *Bulletin of the Seismological Society of America* 113: 2275–2291.

Saint Louis University (2020) SLU regional moment tensors by year. *Saint Louis University Earthquake Center*. Available at: https://www.eas.slu.edu/eqc/eqc_mt/MECH.NA/MECH.NA.2020/20200318130931/HTML.REG/index.html

Savitzky A and Golay MJE (1964) Smoothing and differentiation of data by simplified least squares procedures. *Analytical Chemistry* 36: 1627–1639.

Savran W and Olsen K (2016) Model for small-scale crustal heterogeneity in Los Angeles basin based on inversion of sonic log data. *Geophysical Journal International* 205: 856–863.

University of Utah (2020a) 2020 Magna earthquake sequence catalog. Available at: https://quake.utah.edu/earthquake-information-products/earthquake-catalogs/2020-magna-earthquake-sequence-catalog

University of Utah (2020b) University of Utah Regional Moment Tensor Solutions for the Intermountain West. Available at: https://quake.utah.edu/earthquake-information-products/earthquake-catalogs/Moment-Tensor-Solutions

Wells DL and Coppersmith KJ (1994) New empirical relationships among magnitude, rupture length, rupture width, rupture area, and surface displacement. *Bulletin of the Seismological Society of America* 84: 974–1002.

Withers KB, Olsen KB and Day SM (2015) Memory-efficient simulation of frequency-dependent Q. *Bulletin of the Seismological Society of America* 105: 3129–3142.

Wong I, Silva W, Olig S, Thomas P, Wright D, Ashland FX, Gregor N, Pechmann JC, Dober M, Christenson G and Gerth R (2002) *Earthquake Scenario and Probabilistic Ground Shaking Maps for the Salt Lake City, Utah, Metropolitan Area*. Miscellaneous Publication MP-02-5. Salt Lake City, UT: Utah Geological Survey.

Wong I, Wu Q and Pechmann JC (2021) The 18 March 2020 M 5.7 Magna, Utah, earthquake: Strong-motion data and implications for seismic hazard in the Salt Lake Valley. *Seismological Research Letters* 92: 773–786.

Xu K and Olsen KB (2024) Calibration of nonlinear rheology parameters in the Salt Lake Basin from the March 18, M5.7 Magna, Utah, earthquake sequence records. *Zenodo repository*. DOI: 10.5281/zenodo.10892430.

Youngs R, Swan FH, Power MS and Schwartz DP (2000) *Probabilistic analysis of earthquake ground shaking hazards along the Wasatch Front, Utah, in assessment of regional earthquake hazards and risk along the Wasatch Front, Utah*. Technical report 1500-M. Salt Lake City, UT: U.S. Geological Survey.